Sandwich Preamble for Burst Synchronization

Stefan H. Müller–Weinfurtner

Laboratorium für Nachrichtentechnik, Universität Erlangen–Nürnberg, Cauerstraße 7, D–91058 Erlangen, Germany
Phone: +49 - 9131 - 85 27114, Fax: +49 - 9131 - 85 28919, *e–mail: smueller@LNT.de, http://www.LNT.de/LNT2/*

Abstract— **A "sandwich" repetition preamble (sandamble) with reduced training overhead is introduced and compared to a conventional repetition preamble with respect to frame and frequency synchronization performance in burst transmission. An optimum metric is derived for sandamble detection. The fundamental idea is independent from the specific modulation scheme, but here results for an Orthogonal Frequency–Division Multiplexing (OFDM) system are studied.**

Keywords—**Synchronization, Repetition Preamble, Optimum Metric**

I. Introduction

PACKET–ORIENTED transmission like discontinuous traffic in wireless Asynchronous Transfer Mode (ATM) requires reliable single–shot synchronization. For this purpose, preamble schemes with periodic signal repetitions [1], [2], [3] are often used. Repeated signal structures allow coarse frame synchronization by finding the extremum of an appropriate time–domain metric. A frequency offset estimate can be obtained from the argument of a correlation result. For sake of efficiency, the training data overhead for frame and frequency synchronization is to be kept low.

In this paper, two different types of repetition structures are compared with respect to their synchronization performance. The *preamble* works with contiguous signal segments and the second structure exploits repeated signal segments being separated by user data and is called sandwich preamble or *sandamble*. The optimum metric for synchronization parameter estimation from the sandamble structure is derived.

II. Transmission Model

The discrete–time complex baseband sample of some modulation scheme (e.g., pulse–amplitude modulation or OFDM) is denoted by $s[k]$, where k represents the discrete time. Periodicity in the training structures is symbolized by the triangles in Fig. 1. In the preamble structure shown in Fig. 1a,

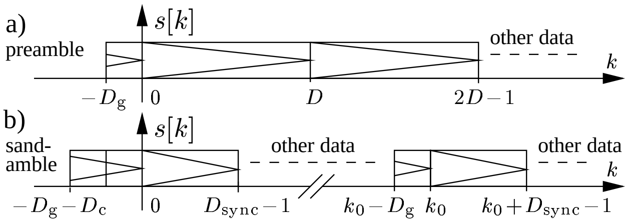

Fig. 1. Transmit signal structure for a) conventional preamble versus b) proposed sandamble (sandwich preamble) with $D_c > 0$.

the training symbols precede the data burst and consist of two identical sample sequences of length D — the first of which starting at discrete–time position $k = 0$. A guard interval (cyclic prefix) of length D_g is added. The sandamble structure shown in Fig. 1b embeds a data symbol sequence, which is not used for training purposes. The signal parts for synchronization consist of two identical symbol sequences of length D_{sync}. Their delay in time direction is k_0 samples and it is clear that now each of the segments requires its own guard interval of D_g samples. The first guard interval is extended by another D_c samples. Hence, the overall sandamble length is $2(D_{sync} + D_g) + D_c$. The burst is usually stored in the receiver memory and demodulated off–line, so that the sandamble structure with embedded data imposes no severe restriction on the system concept. The main reason for the separation is the larger distance of the repeated signal parts, which in turn allows a reduced–variance frequency offset estimation. Further, $D_c > 0$ helps to enlarge the frequency lock–in range and to improve frame synchronization if the ratio of k_0 and D_{sync} is appropriately designed. Note that the preamble becomes a special case of the sandamble for $D_c = 0$ and $k_0 = D_{sync}$.

We consider transmission over a dispersive channel. Hence, the sample sequence $s[k]$ is convolved with the channel impulse response which yields the noiseless receive signal $\tilde{r}_0[k]$. The carrier frequency mismatch is modelled in baseband by modulation of $\tilde{r}_0[k]$ with the absolute carrier frequency offset Δf_{co}. This yields the noiseless received sample $\tilde{r}[k] = \tilde{r}_0[k]\,e^{+j2\pi\Delta f_{co}kT} = \tilde{r}_0[k]\,e^{+j\psi_f k}$, where we introduced the normalized phase velocity (NPV) $\psi_f = 2\pi\Delta f_{co}T$. At the receiver input, samples $n[k]$ of additive white Gaussian noise are added to obtain the received sample $r[k] = \tilde{r}[k] + n[k]$. The average signal power is $\sigma_s^2 = \mathcal{E}\{|s[k]|^2\} = E_s/T$, where E_s is the average received energy per channel symbol. The noise power is $\sigma_n^2 = \mathcal{E}\{|n[k]|^2\} = N_0/T$, where N_0 is the one–sided power spectral density of the white noise. The channel signal–to–noise power ratio (SNR) at the receiver input is $E_s/N_0 = \sigma_s^2/\sigma_n^2$.

III. Standard Synchronization Metric

First, we consider the preamble and the sandamble with $D_c = 0$, only, i.e. without guard extension.

The maximum normalized correlation (MNC) metric [4], [5] for frame synchronization reads

$$\hat{k} = \underset{\tilde{k}}{\operatorname{argmax}} \left(\left| S[\tilde{k}] \right|^2 \Big/ \left(P[\tilde{k}] + P[\tilde{k} + k_0] \right)^2 \right), \qquad (1)$$

where $S[k] = \sum_{\kappa=0}^{D_{sync}-1} r^*[k+\kappa]\, r[k+k_0+\kappa]$ is the complex correlation. $P[k] = \sum_{\kappa=0}^{D_{sync}-1} |r[k+\kappa]|^2$ is the power sum inside a window of D_{sync} received samples. Hence, the correlation is normalized to the overall power sum in the observation window.

Thereafter, the maximum–likelihood (ML) estimate [6] for the NPV can be obtained by evaluating $S[k]$ at the estimated frame start, i.e., $k = \widehat{k}$, and this yields

$$\widehat{\psi_f} = \arg\left(S[\widehat{k}]\right)/k_0. \quad (2)$$

The quality of the NPV estimate $\widehat{\psi_f}$ is evaluated by its variance in the presence of a demodulation window misplacement $D_\mathrm{m} \neq 0$, i.e., $S[\widehat{k}]$ including D_m correlation products which are equivalent to interference. The normalized estimation variance can be calculated as

$$\sigma^2_{\psi_f} \approx \frac{1}{k_0^2 D_\mathrm{sync}\left(1 - D_\mathrm{m}/D_\mathrm{sync}\right)^2} \cdot \cdot \left(\frac{1}{E_s/N_0} + \frac{1}{2(E_s/N_0)^2} + \frac{D_\mathrm{m}/D_\mathrm{sync}}{2}\right). \quad (3)$$

Fig. 2 shows the standard deviation to compare the preamble vs. the sandamble structure. The special scaling expresses the normalization of the estimate to the subcarrier spacing of an OFDM system with $D = 64$. The preamble consists of 136 samples, while the sandamble — with $D_\mathrm{c} = 0$ — occupies 80 modulation intervals, only, but the sandamble performs better than the preamble. More interesting is the behaviour in the presence of a demodulation window misalignment. Here, the sandamble degrades in larger steps, as the ratio of interference samples to useful signal samples is always larger for the sandamble if $D_\mathrm{sync} < D$. But the generally better performance of the sandamble holds up to $D_\mathrm{m} \leq 6$ to provide $D\sigma_{\psi_f}/(2\pi) \leq 10^{-2}$ at SNRs beyond 8 dB. Thus, we expect that the sandamble with the proposed OFDM parameters will exhibit a comparable or even better NPV estimation accuracy and robustness against (residual) time offsets, when compared to the preamble.

Surprisingly, the *frame* synchronization performance is nearly unaffected when reducing the correlation window size from 64 to 32, so that in this respect the larger preamble offers no advantage over the sandamble.

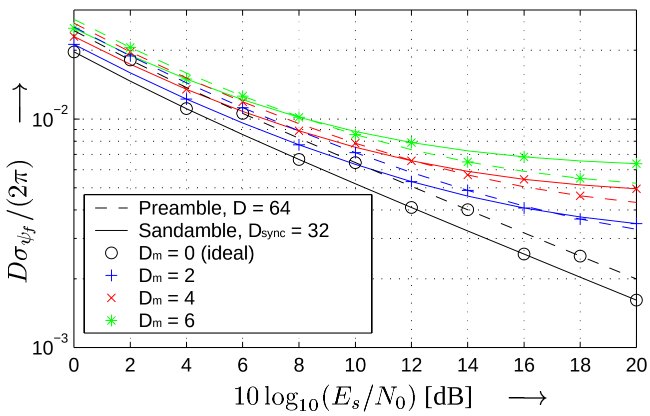

Fig. 2. Normalized frequency estimation standard deviation according to (3) for the preamble ($D = 64$, ATMmobil) and the sandamble ($D_\mathrm{sync} = 32$, $k_0 = 112$) structure in the presence of a misplacement D_m. The fixed OFDM parameters are $D = 64$, $D_\mathrm{g} = 8$.

IV. Optimum Synchronization using Sandamble

We consider the sandamble with *extended* guard interval in Fig. 1b and derive an optimum metric for joint frame and frequency synchronization [5]. Guard extension leads to further periodicity intervals and D_c modulation intervals are additionally exploitable for synchronization, which is advantageous for the accuracy of frame positioning as well as the lock–in range and accuracy of the frequency estimate.

To tackle the problem of optimum frame and frequency synchronization, we collect a sequence of $D_\mathrm{c} + k_0 + D_\mathrm{sync}$ contiguous noisy received samples in the vector $\boldsymbol{r}_k = [r[k-D_\mathrm{c}], \ldots, r[k+k_0+D_\mathrm{sync}-1]]^\mathsf{T}$. This sample vector comprises the entire range of exploitable knowledge on sample periodicity in the sandamble. The (non–observable) noiseless received samples $\tilde{r}[k]$ are collected in $\tilde{\boldsymbol{r}}_k$. Finally, with definition of the channel noise vector $\boldsymbol{n}_k = [n[k-D_\mathrm{c}], \ldots, n[k+k_0+D_\mathrm{sync}-1]]^\mathsf{T}$ of dimension $D_\mathrm{c} + k_0 + D_\mathrm{sync}$, the relation $\boldsymbol{r}_k = \tilde{\boldsymbol{r}}_k + \boldsymbol{n}_k$ is valid.

Obviously, there are at least two different periodicity intervals which can be exploited. Firstly, the main part of length D_sync exhibits a periodicity spacing of k_0 modulation intervals. For this main repetition part, the $D_\mathrm{sync} \times (D_\mathrm{c} + k_0 + D_\mathrm{sync})$ masking matrices[1]

$$\boldsymbol{M}_\mathrm{m} = \left[\boldsymbol{0}_{D_\mathrm{sync}\times D_\mathrm{c}} \; \boldsymbol{I}_{D_\mathrm{sync}} \; \boldsymbol{0}_{D_\mathrm{sync}\times k_0}\right] \quad (4)$$

$$\boldsymbol{B}_\mathrm{m} = \left[\boldsymbol{0}_{D_\mathrm{sync}\times (D_\mathrm{c}+k_0)} \; \boldsymbol{I}_{D_\mathrm{sync}}\right] \quad (5)$$

are introduced. Secondly, the extended guard interval allows the exploitation of a periodicity spacing of D_sync modulation intervals in a region of length D_c. To account for the periodicity due to this guard interval extension, the masking matrices

$$\boldsymbol{M}_\mathrm{x} = \left[\boldsymbol{0}_{D_\mathrm{c}\times D_\mathrm{sync}} \; \boldsymbol{I}_{D_\mathrm{c}} \; \boldsymbol{0}_{D_\mathrm{c}\times k_0}\right] \quad (6)$$

$$\boldsymbol{B}_\mathrm{x} = \left[\boldsymbol{I}_{D_\mathrm{c}} \; \boldsymbol{0}_{D_\mathrm{c}\times (k_0+D_\mathrm{sync})}\right], \quad (7)$$

both of dimension $D_\mathrm{c} \times (D_\mathrm{c} + k_0 + D_\mathrm{sync})$, are defined. Note that $\boldsymbol{M}_\mathrm{x}$ and $\boldsymbol{B}_\mathrm{x}$ disappear for $D_\mathrm{c} = 0$, as they collapse to dimension zero. Furthermore, the matrix

$$\boldsymbol{E}_{\psi_f} \triangleq \begin{bmatrix} \mathrm{e}^{+\mathrm{j}k_0\psi_f}\boldsymbol{M}_\mathrm{m} - \boldsymbol{B}_\mathrm{m} \\ \mathrm{e}^{-\mathrm{j}D_\mathrm{sync}\psi_f}\boldsymbol{M}_\mathrm{x} - \boldsymbol{B}_\mathrm{x} \end{bmatrix} \quad (8)$$

is introduced, which incorporates the phase relation of the repeated structures for some NPV ψ_f. Due to the known structure and known periodicity intervals, it is exploitable that the noiseless vector $\tilde{\boldsymbol{r}}_k$ at the correct timing instant $k = 0$ fulfills

$$\boldsymbol{E}_{\psi_f}\tilde{\boldsymbol{r}}_0 = \boldsymbol{0}, \quad (9)$$

where $\boldsymbol{0}$ is the all–zero vector. To derive a criterion for synchronization based on the above identity, the error vector

$$\boldsymbol{e}_{\tilde{k},\tilde{\psi}_f} \triangleq \boldsymbol{E}_{\tilde{\psi}_f}\boldsymbol{r}_{\tilde{k}} \quad (10)$$

is introduced. This vector depends on the frame start hypothesis $\tilde{k}$ and the NPV hypothesis $\tilde{\psi}_f$. It can be shown that

$$\boldsymbol{e}_{\tilde{k},\tilde{\psi}_f} = \begin{bmatrix} \mathrm{e}^{+\mathrm{j}k_0\psi_f}\boldsymbol{M}_\mathrm{m} - \boldsymbol{B}_\mathrm{m} \\ \mathrm{e}^{-\mathrm{j}D_\mathrm{sync}\psi_f}\boldsymbol{M}_\mathrm{x} - \boldsymbol{B}_\mathrm{x} \end{bmatrix}\left((\tilde{\boldsymbol{r}}_{\tilde{k}} - \tilde{\boldsymbol{r}}_0) + \boldsymbol{n}_{\tilde{k}}\right) + \begin{bmatrix} (\mathrm{e}^{+\mathrm{j}k_0\tilde{\psi}_f} - \mathrm{e}^{+\mathrm{j}k_0\psi_f})\boldsymbol{M}_\mathrm{m} \\ (\mathrm{e}^{-\mathrm{j}D_\mathrm{sync}\tilde{\psi}_f} - \mathrm{e}^{-\mathrm{j}D_\mathrm{sync}\psi_f})\boldsymbol{M}_\mathrm{x} \end{bmatrix}\boldsymbol{r}_{\tilde{k}}, \quad (11)$$

[1] $\boldsymbol{0}$ and $\boldsymbol{I}$ are zero and identity matrices of given size, respectively.

where the first component is mainly determined by the difference vector of time–shifted received sample sequences, while the second is influenced by a matrix which becomes all–zero for $\tilde{\psi}_f = \psi_f$. For the case of perfect synchronization trial variables $\tilde{\psi}_f = \psi_f$ and $\tilde{k} = 0$, the error vector is purely determined[2] by

$$\boldsymbol{e}_{\tilde{k},\tilde{\psi}_f} = \boldsymbol{E}_{\tilde{\psi}_f} \boldsymbol{n}_{\tilde{k}}. \tag{12}$$

Synchronization shall be based on maximizing the probability density $p_{\boldsymbol{e}}(\boldsymbol{e}_{\tilde{k},\tilde{\psi}_f} \mid \tilde{\psi}_f = \psi_f, \tilde{k} = 0)$ of the structure–defined similarity in the sample sequence. For white Gaussian channel noise, the covariance matrix of $\boldsymbol{e}_{\tilde{k},\tilde{\psi}_f}$ is $\sigma_n^2 \boldsymbol{E}_{\tilde{\psi}_f} \boldsymbol{E}^{\mathsf{H}}_{\tilde{\psi}_f}$, where $(\cdot)^{\mathsf{H}}$ denotes the (complex) conjugate transpose of a vector/matrix. Hence, the synchronizer aims to find the optimum tuple

$$\begin{aligned} [\,\widehat{k}, \widehat{\psi_f}\,] &= \underset{[\,\tilde{k},\tilde{\psi}_f\,]}{\operatorname{argmin}}\; \boldsymbol{e}^{\mathsf{H}}_{\tilde{k},\tilde{\psi}_f} \left(\sigma_n^2 \boldsymbol{E}_{\tilde{\psi}_f} \boldsymbol{E}^{\mathsf{H}}_{\tilde{\psi}_f}\right)^{-1} \boldsymbol{e}_{\tilde{k},\tilde{\psi}_f} \\ &= \underset{[\,\tilde{k},\tilde{\psi}_f\,]}{\operatorname{argmin}}\; \boldsymbol{r}^{\mathsf{H}}_{\tilde{k}} \boldsymbol{C}_{\tilde{\psi}_f} \boldsymbol{r}_{\tilde{k}}, \end{aligned} \tag{13}$$

where the optimum[3] synchronization correlation matrix is introduced as

$$\boldsymbol{C}_{\tilde{\psi}_f} \stackrel{\triangle}{=} \boldsymbol{E}^{\mathsf{H}}_{\tilde{\psi}_f} \left(\boldsymbol{E}_{\tilde{\psi}_f} \boldsymbol{E}^{\mathsf{H}}_{\tilde{\psi}_f}\right)^{-1} \boldsymbol{E}_{\tilde{\psi}_f}. \tag{14}$$

This matrix is obviously Hermitian symmetric, and furthermore, it evaluates to a banded structure. The final result for $\boldsymbol{C}_{\tilde{\psi}_f}$ is depicted in Fig. 3. It is worth noting that the periodicity interval $k_0 + D_{\mathrm{sync}}$ appears explicitly in $\boldsymbol{C}_{\tilde{\psi}_f}$, even though (8) and (9) express this periodicity spacing implicitly, only.

The Hermitian banded matrix $\boldsymbol{C}_{\tilde{\psi}_f}$ is partitioned into a diagonal matrix $\boldsymbol{P}$ and the upper triangular matrix $\boldsymbol{F}_{\tilde{\psi}_f}$ such that

$$\boldsymbol{C}_{\tilde{\psi}_f} = \boldsymbol{P} - \boldsymbol{F}_{\tilde{\psi}_f} - \boldsymbol{F}^{\mathsf{H}}_{\tilde{\psi}_f}. \tag{15}$$

The real–valued entries of $\boldsymbol{P}$ represent the diagonal line of $\boldsymbol{C}_{\tilde{\psi}_f}$ in Fig. 3 (see decomposition sketch) and the entries of $\boldsymbol{F}_{\tilde{\psi}_f}$ follow from the upper right triangle via negation. With this partitioning, the synchronization rule (13) is rewritten to obtain the X–MMSE metric (guard–extended minimum mean–squared error)

$$\begin{aligned} [\,\widehat{k}, \widehat{\psi_f}\,] &= \underset{[\,\tilde{k},\tilde{\psi}_f\,]}{\operatorname{argmin}} \Big(\boldsymbol{r}^{\mathsf{H}}_{\tilde{k}} \boldsymbol{P} \boldsymbol{r}_{\tilde{k}} - 2\,\Re\{\boldsymbol{r}^{\mathsf{H}}_{\tilde{k}} \boldsymbol{F}_{\tilde{\psi}_f} \boldsymbol{r}_{\tilde{k}}\} \Big) \\ &= \underset{[\,\tilde{k},\tilde{\psi}_f\,]}{\operatorname{argmin}} \Big(\boldsymbol{r}^{\mathsf{H}}_{\tilde{k}} \boldsymbol{P} \boldsymbol{r}_{\tilde{k}} - 2\,\Re\{C(\tilde{k},\tilde{\psi}_f)\} \Big), \end{aligned} \tag{16}$$

where the expression $\boldsymbol{r}^{\mathsf{H}}_{\tilde{k}} \boldsymbol{P} \boldsymbol{r}_{\tilde{k}}$ is a generalized power sum, while $C(\tilde{k},\tilde{\psi}_f) = \boldsymbol{r}^{\mathsf{H}}_{\tilde{k}} \boldsymbol{F}_{\tilde{\psi}_f} \boldsymbol{r}_{\tilde{k}}$ represents the generalized derotated correlations.

[2]Note that the combination $\tilde{\psi}_f = \psi_f$ and $\tilde{k} = 0$ is not the only combination of values which produces this result. There may be ambiguities for $\tilde{k}$ in proximity of the optimum and for $\tilde{\psi}_f$ in periodic intervals.

[3]This matrix is optimum for white Gaussian channel noise, only.

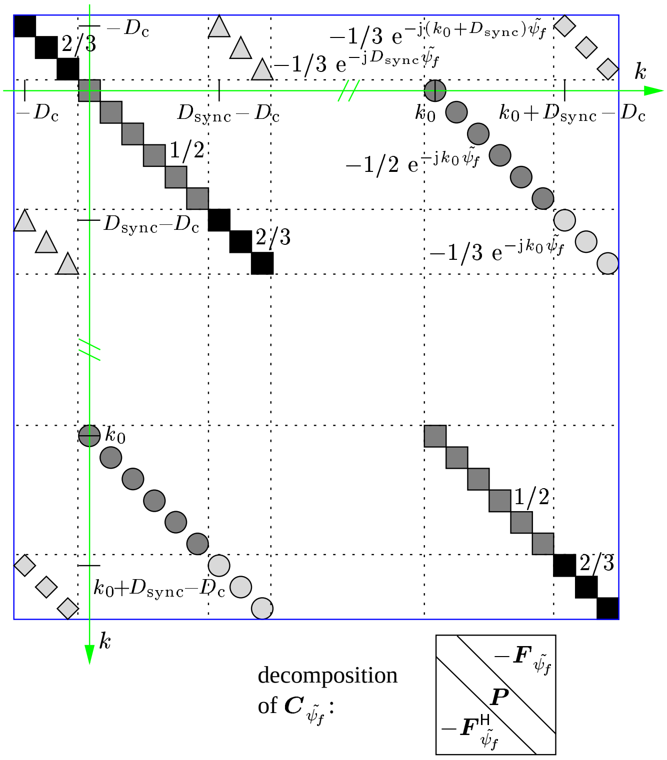

Fig. 3. Optimum correlation matrix $\boldsymbol{C}_{\tilde{\psi}_f}$ to estimate synchronization parameters from an example sandamble with parameters $D_{\mathrm{sync}} = 9$ and $D_{\mathrm{c}} = 3$ in white channel noise. The non–zero matrix entries are indicated by symbols. The degree of shading expresses the magnitude, while the symbol shape characterizes the phase angle. Note that $\boldsymbol{C}_{\tilde{\psi}_f} = \boldsymbol{C}^{\mathsf{H}}_{\tilde{\psi}_f}$. The decomposition $\boldsymbol{C}_{\tilde{\psi}_f} = \boldsymbol{P} - \boldsymbol{F}_{\tilde{\psi}_f} - \boldsymbol{F}^{\mathsf{H}}_{\tilde{\psi}_f}$ is sketched below.

The special banded structure of $\boldsymbol{F}_{\tilde{\psi}_f}$ allows the final partitioning step

$$\boldsymbol{F}_{\tilde{\psi}_f} = \mathrm{e}^{-\mathrm{j}k_0\tilde{\psi}_f}\boldsymbol{S} + \mathrm{e}^{-\mathrm{j}D_{\mathrm{sync}}\tilde{\psi}_f}\boldsymbol{X}_1 + \mathrm{e}^{-\mathrm{j}(k_0+D_{\mathrm{sync}})\tilde{\psi}_f}\boldsymbol{X}_2, \tag{17}$$

where the matrices $\boldsymbol{S}$, $\boldsymbol{X}_1$ and $\boldsymbol{X}_2$ are real–valued and consist of the correlation weighting factors in *one* respective diagonal band, only. Considering the symbols in the upper triangle of the matrix in Fig. 3, the circles of the main correlation belong to $\boldsymbol{S}$, the triangles and the diamonds of the extension correlations to $\boldsymbol{X}_1$ and $\boldsymbol{X}_2$, respectively. Already from the first partitioning (15) follows that the squares belong to $\boldsymbol{P}$. Hence, we obtain the generalized derotated correlation

$$\begin{aligned} C(\tilde{k},\tilde{\psi}_f) \stackrel{\triangle}{=}\; & \mathrm{e}^{-\mathrm{j}k_0\tilde{\psi}_f} \boldsymbol{r}^{\mathsf{H}}_{\tilde{k}} \boldsymbol{S} \boldsymbol{r}_{\tilde{k}} + \mathrm{e}^{-\mathrm{j}D_{\mathrm{sync}}\tilde{\psi}_f} \boldsymbol{r}^{\mathsf{H}}_{\tilde{k}} \boldsymbol{X}_1 \boldsymbol{r}_{\tilde{k}} \\ & + \mathrm{e}^{-\mathrm{j}(k_0+D_{\mathrm{sync}})\tilde{\psi}_f} \boldsymbol{r}^{\mathsf{H}}_{\tilde{k}} \boldsymbol{X}_2 \boldsymbol{r}_{\tilde{k}}. \end{aligned} \tag{18}$$

Further, it is advantageous to maximize the X–MNC metric $M_{\mathrm{opt}}[k,\psi_f] = 2\,\Re\{C(\tilde{k},\tilde{\psi}_f)\}/\boldsymbol{r}^{\mathsf{H}}_{\tilde{k}} \boldsymbol{P} \boldsymbol{r}_{\tilde{k}}$, which reads

$$[\,\widehat{k}, \widehat{\psi_f}\,] = \underset{[\,\tilde{k},\tilde{\psi}_f\,]}{\operatorname{argmax}} \frac{2\,\Re\{C(\tilde{k},\tilde{\psi}_f)\}}{\boldsymbol{r}^{\mathsf{H}}_{\tilde{k}} \boldsymbol{P} \boldsymbol{r}_{\tilde{k}}} = \underset{[\,\tilde{k},\tilde{\psi}_f\,]}{\operatorname{argmax}}\; M_{\mathrm{opt}}[\tilde{k},\tilde{\psi}_f]. \tag{19}$$

The denominator (matrix $\boldsymbol{P}$) serves as generalized power normalization, while the nominator (matrices $\boldsymbol{S}$, $\boldsymbol{X}_1$, and $\boldsymbol{X}_2$) represent the correlation contributions.

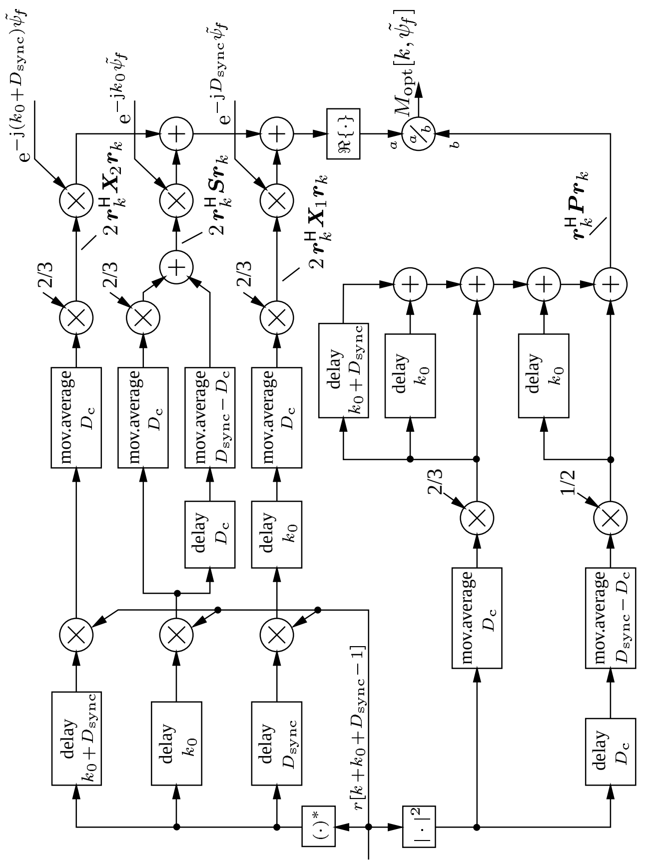

Fig. 4. Implementation of optimum joint frame and frequency synchronization metric X–MNC for detection of a sandamble with extended guard interval. If the NPV is not known, the metric needs to be maximized in each time step over the NPV trial variable (hypothesis) $\tilde{\psi}_f$.

Fig. 4 shows an implementation of the X–MNC metric for joint frequency and frame synchronization. The block diagram shows the calculation of the synchronization metric in each modulation cycle as function of the NPV hypothesis $\tilde{\psi}_f$. Not depicted here is that in each step an optimum hypothesis $\widehat{\psi_f}$ needs to be determined. A near–optimum approximate solution is derived in [5].

V. Simulation Results for Sandamble

The optimum X–MNC metric from (19) is compared via simulation to the simpler MNC metric from (1), which disregards the guard interval extension. The assumed simulation scenario includes a sandamble with $D_c = 8$ samples in the extended guard interval, a symbol size of $D_{sync} = 32$ embedded between two random OFDM symbols with $D = 64$ and the same average power as during the sandamble. The data OFDM symbol in–between the two sandamble parts is also random. No silent periods are present within the available signal interval. Lock–in histograms for the MNC and X–MNC frame synchronization metrics in a dispersive channel with exponential power delay profile are given in Fig. 5. The benefit of the additional structure knowledge of $D_c = 8$ samples in X–MNC is tremendous as the lock–in behaviour is much more pronounced in proximity of the correct timing instant; false locks outside the preamble region are easily reduced by a order of magnitude.

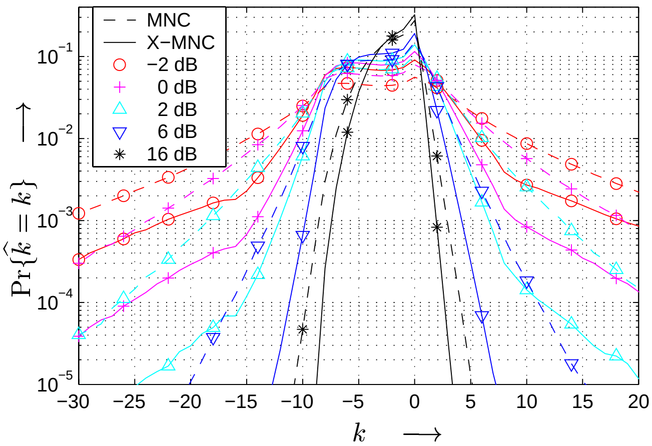

Fig. 5. Simulation results for the lock–in probabilities achieved with the sandamble ($D_{sync} = 32$, $D_c = 8$) in a dispersive channel. The simulations are performed for various $10\log_{10}(E_s/N_0)$ [dB] to compare the frame synchronization metrics in (1) and (19).

VI. Summary and Conclusions

We introduced the sandwich repetition preamble (sandamble) scheme, derived an optimum synchronization metric, and compared its performance to a standard repetition preamble. We outlined the advantage of the sandamble in terms of burst overhead vs. frame and frequency synchronization accuracy. An appropriately designed sandamble structure offers immense flexibility to trade frequency lock–in range against estimation robustness and burst overhead for synchronization [5].

Acknowledgement

This work was supported by Ericsson Eurolab Deutschland GmbH in Nürnberg and is funded in parts by the national research initiative ATMmobil of the German Ministry for Research and Education (BMBF).

The author thanks Prof. J. Huber for fruitful discussions.

References

[1] Pierre R. Chevillat, Dietrich Maiwald, and Gottfried Ungerboeck, "Rapid Training of a Voiceband Data–Modem Receiver Employing an Equalizer with Fractional–T Spaced Coefficients," *IEEE Trans. on Commun.*, vol. 35, no. 9, pp. 869–876, 1987.

[2] Timothy M. Schmidl and Donald C. Cox, "Robust Frequency and Timing Synchronization for OFDM," *IEEE Trans. on Commun.*, vol. 45, no. 12, pp. 1613–1621, 1997.

[3] Michael Speth, Ferdinand Classen, and Heinrich Meyr, "Frame synchronization of OFDM systems in frequency selective fading channels," in *Proceedings of IEEE Vehicular Technology Conference (VTC'97)*, Phoenix, Arizona, USA, 1997, pp. 1807–1811.

[4] Andreas Czylwik, "Low Overhead Pilot–Aided Synchronization for Single Carrier Modulation with Frequency Domain Equalization," in *Proceedings of IEEE Global Telecommunications Conference (GLOBECOM'98)*, Sydney, Australia, November 1998, pp. 2068–2073.

[5] Stefan Müller–Weinfurtner, *OFDM for Wireless Communications: Nyquist Windowing, Peak–Power Reduction, and Synchronization*, Reihe Kommunikations- und Informationstechnik, Band 16, ISBN 3-8265-7658-6. Shaker Verlag, Aachen, 2000, Dissertation Universität Erlangen–Nürnberg.

[6] Jan-Jaap van de Beek, Magnus Sandell, and Per Ola Börjesson, *ML Estimation of Timing and Frequency Offset in Multicarrier Systems*, Research report. Div. of Signal Processing, Luleå University of Technology, Sweden, 1996.